Chapter III

Temperature Dependent Electron Spin Relaxation in Cupric and Vanadyl Phthalocyanines

Introduction

Quantum information science (QIS) is a growing field that encompasses a range of technologies that take advantage of quantum properties such as coherence and entanglement. These technologies include quantum computing, cryptography, as well as quantum sensing and metrology.[1] These applications broadly regard the writing, reading, and transfer of information in some form. The fundamental unit of information in QIS is the quantum bit or "qubit." In contrast to classical computation, in which a bit can occupy a 0 or 1 state, the qubit may be initiated into a coherent superposition of the two states, which can be described by any linear combination of the basis states (i.e. $\alpha|0\rangle + \beta|1\rangle$ where α and β are, in general, complex numerical constants and by typical convention $|\alpha|^2 + |\beta|^2 = 1$). For a single qubit, states can be represented by a vector on a unit sphere, known as a Bloch sphere, as shown in Figure 3.1.

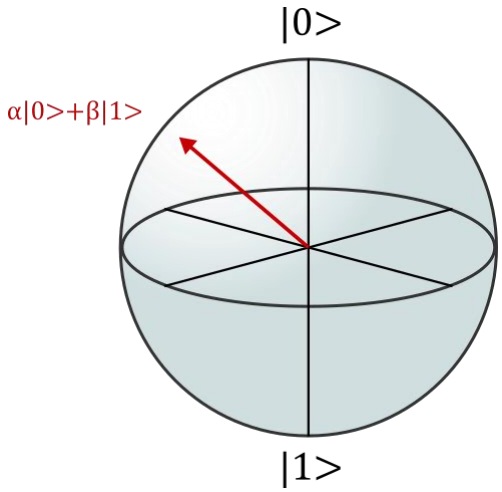

Figure 3.1 The Bloch sphere representation of an arbitrary superposition state $\alpha|0\rangle + \beta|1\rangle$.

The ability to parallelize qubits in superposition states provides quantum algorithms benefits over classical algorithms when applied to certain types of problems. Quantum

computation may promise enhanced speed when it comes to factoring large numbers (e.g., Shor's algorithm), searching databases, and simulating quantum systems among other problems that pose challenges to classical computing architectures.

In 2000, DiVincenzo put forth a set of rules for the implementation of a qubit in a quantum computing framework: (1) the physical system implementing the qubits should be scalable and the qubits themselves well-defined, (2) the qubit should be readily initialized into a simple initial state, (3) the qubit should exhibit a long coherence lifetime within which operations can be performed, (4) there must be universally applicable quantum gates or operations to perform on the qubit system, and (5) each qubit should be individually addressable. These guidelines have availed researchers in the field toward fundamental understanding and implementation of quantum information systems.[1]

A qubit, by the definition given above, represents any quantum object encompassing a two-level system. This could be the spin states of an S = ½ particle, the vertical and horizontal polarizations of a photon, the quantized flux, charge, or phase states of designed superconducting loops, or the ground and excited electronic states of an atom or molecule.[2–4] Particularly in the case of molecular systems, there are generally many more available spin and electronic states than two. However, we often treat a given transition by considering just two states (an upper and lower) when they are separated by an energy that is resonant with an external radiation field. If the coupling of the two qubit states to the other internal states of the system remains small, the case when the other states are disparate in energy from the relevant states, the two-level system approximation holds. Efforts have been made to describe individual qubits with greater than two levels. Although sometimes named with respect to the number of states in the manifold, such systems are often collectively referred to as "qudits," regardless of the number of states.

Each type of qubit candidate has both advantages and disadvantages for its implementation in QIS architectures. For example, superconducting qubit circuits are macroscopic objects that behave quantum mechanically and can be manufactured by photo- or electron-beam lithography. Superconducting qubits allow for tailoring of resonant frequencies and interqubit coupling. Single qubits may also be addressed by application of external electric or microwave fields. However, superconducting qubits typically require exceptionally low temperatures (often milli-Kelvin ranges) for successful operation and protection from decoherence. This poses a challenge to scalability as well as high operational costs due to the refrigerator requirement.[2] Qubits based on nuclear or electronic spin can boast long coherence lifetimes and may be robust to decoherence at higher temperatures, which may aid in scalability and operational costs. However, the energy levels of single atom spin systems cannot readily be tuned as they are intrinsic to the atom. Atomic spin defects in solid-state semiconductors have long been proposed as a potential platform for QIS and systems such as P defects in SiC or N-vacancy centers in diamond have found important applications.[5–9] Still, tailorability of individual qubit Hamiltonian parameters, control of qubit placement within the material, and control of interqubit interaction remains challenging. Molecular spin qubits have therefore garnered attention for the ability to tune the Hamiltonian of a given spin system as well as to control qubit-qubit spacing and coupling by synthetic design.[3,4]

For an electron spin qubit in an externally applied magnetic field, the system may be initialized and operated on by a microwave pulse resonant with the Zeeman splitting of the spin sublevels. The states of the system may therefore be read out via pulsed electron paramagnetic resonance (EPR) spectroscopy.[10–21] In EPR, the bulk magnetization of the sample is measured. Once the net magnetization is rotated from its alignment with the external field by the microwave pulse, the system will reapproach equilibrium via magnetic relaxation pathways. The important

magnetic relaxation parameters are the spin-lattice or longitudinal relaxation time (T_1) and the spin-spin or phase memory time (T_M) (see Introduction for further information on T_1 and T_M).

The phase memory time, and more specifically T_2, report on the decoherence time of the qubit system. It has been estimated that T_2 lifetimes greater than 100 μs are necessary to perform desired gate sequences using a qubit. However, in pursuit of qubit technologies approaching room temperature, we must also consider the spin-lattice relaxation behavior of the system. At low temperatures, the T_1 time is generally much longer than the T_M. However, as the temperature increases, the T_1 time will decrease, often rapidly so. As the T_1 time reflects the return of the z-component of the magnetization vector, this also forces the transverse components to zero, limiting the ability to manipulate and read out coherence. It is this regime in which we describe T_M as being T_1-limited and is the focus of the current study.[22,23]

Here we examine two S = ½ metal complexes in the context of their magnetic relaxation properties as it pertains to quantum information science: Cu(II) phthalocyanine (CuPc) and vanadyl (VOPc) phthalocyanine.[24–27] The temperature-dependent magnetic relaxation behavior of VOPc was previously characterized in various dilutions in diamagnetic titanyl phthalocyanine (TiOPc) matrices by Atzori et al.[14] These works stand in a long line of investigation into paramagnetic relaxation processes in inorganic coordination complexes. The foundational theory of spin-lattice relaxation was laid by Van Vleck, Pryce, Orbach, and others. G. R. and S. S. Eaton have further expanded the experimental study of orientation-, field-, and temperature-dependent magnetic relaxation in organic and inorganic systems.[23,28–37]

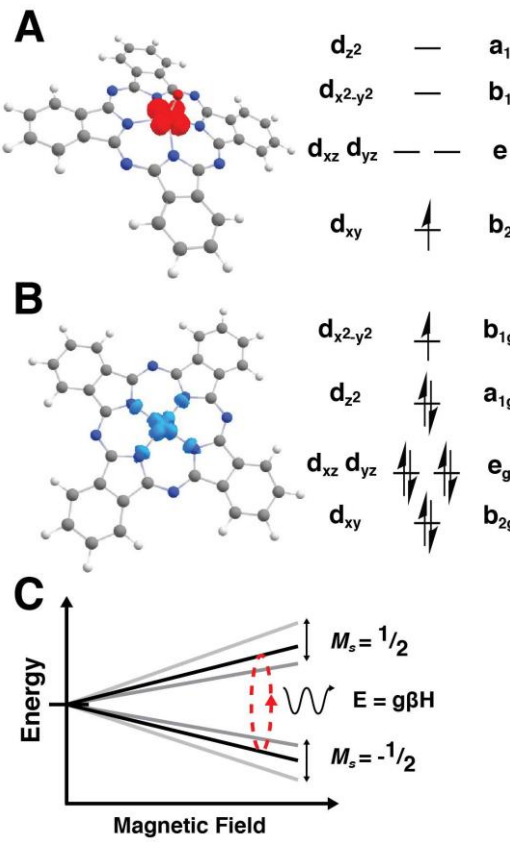

Figure 3.2 Spin densities and qualitative 3d-orbital energy diagrams for (**A**) VOPc and (**B**) CuPc. (**C**) Zeeman splitting of the M_s sublevels of an S = ½ system and the effects of spin-phonon-induced modulation of the energy splitting (gray lines) and coherence (red-dashed ellipse).

Results

According to prior literature, we prepared polycrystalline samples of VOPc diluted in a diamagnetic TiOPc matrix at 1:1000 and 1:100 VOPc/TiOPc concentrations. We examined the PXRD patterns of both mixtures and found them to be consistent with previously reported data for the type II polymorph. We collected the X-band CW EPR spectra for each sample and they are consistent with each other, exhibiting the expected eight-line powder pattern for V^{IV} (the almost 100% naturally abundant ^{51}V has a nuclear spin I = 7/2). Notably, these spectra also feature the presence of an additional isotropic EPR transition centered around g ~ 2, consistent with an organic

radical. Such radical impurities have commonly been observed in metal- and metal-free phthalocyanine EPR spectra. Echo-detected field sweeps (EDFSs) of the two samples taken at 5 and 60 K are likewise consistent with previous reports. The EDFS, T_1 inversion recovery, and T_m Hahn echo sequences were collected across a range of temperatures from 5 – 300 K for both samples.

Orientation Dependence of T_1 and T_m in VOPc

We compare here the T_1 and T_m times estimated from inversion recovery and two pulse Hahn echo experiments collected at four magnetic field positions, 303 ($g_{||}$, $M_I = -5/2$), 329 ($g_{\perp}$, $M_I = -3/2$), 335.6 ($g_{||}$ and $g_{\perp}$, $M_I = -1/2$), and 386 mT ($g_{||}$, $M_I = +5/2$) at X-band. We carried out identical experiments at four magnetic field positions at Q-band: 1197.5 ($g_{||}$, $M_I = -5/2$), 1214 ($g_{\perp}$, $M_I = -3/2$), 1218 ($g_{\perp}$, $M_I = -1/2$), and 1265.5 mT ($g_{||}$, $M_I = +5/2$). The assignments of the M_I eigenvalues involved in the transitions are kept consistent with Du et al. We chose these magnetic field positions to sample a variety of resonance conditions near extrema for parallel and perpendicular orientations to the field and various hyperfine sublevels.

There is a small observable orientation dependence of T_1 in 1:1000 VOPc at X-band, but it remains across the temperature range sampled. We observe slightly longer T_1 times on the wings of the spectrum at the peaks associated with the $M_I = -5/2$ and $+5/2$ transitions of $g_{||}$, although there is overall little differentiation between M_I sublevel transitions.[35] We observe a similar orientation dependence on T_1, although there is an unexpected rise in the T_1 times collected at the 1218 mT feature at 110 K. Although this rise was reproducible, we are as yet unsure of its origin.

There is a slight orientation dependence in the T_m values as well, and we similarly observe the parallel extrema of the $M_I = -5/2$ and $+5/2$ having longer T_m times than at the perpendicular

positions. The sensitivity of T_m's to orientation has been previously ascribed to molecular motions, particularly those that can move a given spin system out of resonance with the microwave pulse that ultimately refocuses the spin packet, as this leads to decoherence. For an axial system such as VOPc, it is convenient to consider the molecular z-axis and its orientation relative to the B_0 field of the spectrometer. Owing to the anisotropy of the spin system, the resonant magnetic field changes upon rotating the molecular z-axis away from parallel to perpendicular orientations with respect to the external field. Importantly, the resonant field changes more rapidly with the rotation angle nearing perpendicular orientations. This contextualizes the orientation dependence of T_m observed as low frequency motions will impact the resonance field of a spin system near perpendicular orientations, leading to greater decoherence, more so than at parallel orientations. For example, in CuTTP and VOTTP (TTP = 5,10,15,20-tetratolylporphyrin), the phase memory times declined as the applied field approaches resonant conditions with intermediate orientations.[23] Due to the axial nature of VOPc and CuPc, we therefore expect that out-of-plane motions that disturb the transition metal center will be most relevant for shortening T_m's at a given position.

Frequency Dependence of T_1 and T_m in VOPc

At Q-band, the EDFS spectra of VOPc exhibit sharper features than at X-band owing to the better resolved vanadium hyperfine transitions. We observe these same transitions across the 5 to 300 K range in the EDFSs. The trends in T_1's and T_m's across the temperature range are similar to those observed at X-band. Although the T_1 trend is similar at each field position at X-band, the T_1's obtained at 1218 mT are notably longer than those measured at other positions throughout the temperatures examined. Previous reports examined the relaxation behavior of VOTTP-COOH (TTP-COOH = 5-(4-carboxyphenyl)-10,15,20,-tri(tolyl)porphyrin) at S-, X-, and W-band and found that at higher temperatures the T_1's become similar irrespective of the spectrometer

frequency. We similarly observe this trend in T_1's above 50 K in our VOPc samples. In this temperature range, Raman and local mode mechanisms may dominate spin-lattice relaxation, and these pathways are expected to be frequency-independent. At low temperatures, as is observed for VOTTP-COOH, direct processes dominate relaxation and give rise to faster relaxation rates going from S- to X- to W-band.[36] The direct process is proportional to B_0^4 for a Kramers system.[37] We observe, overall, quite comparable T_1 times between our VOPc data collected at X-band versus Q-band.

The T_m times follow a similar pattern observed for T_1 in that the phase memory times measured at 1218 mT were markedly longer than those measured at other field positions at Q-band. The T_m's measured at 1218 mT at Q-band were comparable to those measured in the X-band experiments, whereas the T_m's collected at other positions measured at Q-band were generally shorter than the corresponding times measured at X-band.

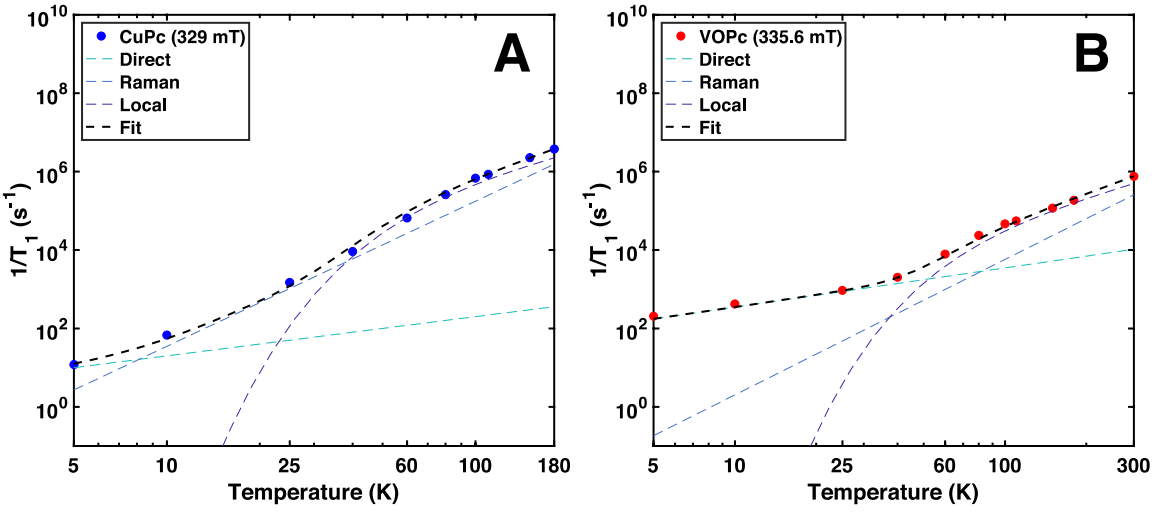

Figure 3.3 Fits of the temperature dependence of $1/T_1$ vs. temperature to direct, Raman, and local mode processes for (A) CuPc (329 mT) and (B) VOPc (335.6 mT) 1:1000 preparations at X-band.

Temperature Dependence of T_1 and T_m in VOPc

Atzori et al. reported spin-lattice relaxation times of the 1:1000 VOPc/TiOPc samples to be 14 ms at 4.3 K, 0.22 ms at 40 K, and 1.1 μs at 300 K. Across the field positions sampled, we found comparable T_1 relaxation times of 3.3-9.6 ms at 5 K, 0.38 – 0.64 ms at 40 K, and 0.84 – 2.9 μs at 300 K. The T_1 temperature dependence of VOPc in 0.5 mM D_2SO_4 solution was previously studied and exhibited a T_1 of 45 μs at 99 K.[26] In general, we observe shorter T_1's in the 1:100 VOPc sample compared to the 1:1000 dilution. This is consistent with higher concentrations of the paramagnetic center leading to greater spin-spin mediated relaxation.

We fit the temperature-dependent spin-lattice relaxation rates of 1:1000 VOPc/TiOPc measured at 335.6 mT at X-band as shown in Figure 3.3. This sharp, near-isotropic lineshape at 335.6 mT is a result of the coincidence of the perpendicular and parallel resonances in the $M_I = -1/2$ hyperfine sublevel and is referred to as the "powder-position" in vanadyl-systems.[38] We fit the data to a direct, Raman, and local mode process using Appendix B Eq. B5 (more information regarding fitting is found in Appendix B).[33] The fitted parameters are given in Table 1. For VOPc, we determined a direct process coefficient A_{dir} = 35 K^{-1} s^{-1}) which dominates at low temperature, a Raman contribution with coefficient B_{ram} = 1.1 x 10^4 s^{-1} and Debye temperature θ_D = 119.6 K, and local mode contribution with coefficient C_{loc} = 5.2 x 10^5 s^{-1} and effective mode temperature Δ_{loc} = 295.1 K). We focused our sampling in the high temperature range as we are principally interested in the regime where T_m becomes T_1-limited. Undersampling in the low temperature limit likely leads to a poor estimation of the direct coefficient. That said, the parameters we obtained are in good agreement with similar fits reported for VOTTP doped in diamagnetic ZnTTP (A_{dir} = 11.5 K^{-1} s^{-1}, B_{ram} = 1.1 x 10^4 s^{-1}, θ_D = 100 K, C_{loc} = 4.0 x 10^5 s^{-1}, Δ_{loc} = 350 K).[33]

Table 3.1. Fitting parameters of the 1:1000 CuPc and VOPc samples at X-band for direct (A_{dir}), Raman (B_{ram}), local mode coefficients (C_{loc}) as well as the Deby temperature (θ_D) and power dependence of Raman (n) and local mode activation energy (Δ_{loc})

	CuPc (329 mT)	VOPc (335.6 mT)
A_{dir} ($K^{-1}s^{-1}$)	2	35
B_{ram} (s^{-1})	$2.732 \cdot 10^5$	$1.069 \cdot 10^4$
C_{loc} (s^{-1})	$6.201 \cdot 10^6$	$5.226 \cdot 10^5$
θ_D (K)	112.8	119.6
n	3.7	3.455
Δ_{loc} (K)	272.1	295.1

The temperature dependence of T_m is relatively small until it becomes T_1 limited near 300 K.[39] The 1:1000 sample showed largely temperature-independent T_m's ranging from 2.0 to 2.5 μs across all field positions between 5 and 150 K, decreasing to 1.38 and 1.46 μs at 329 and 335.6 mT, respectively, at 300 K, which is consistent with the previous report from Atzori et al. For all field positions, we find a maximum phase memory time near 40 K. Increasing the temperature from 40 K, there is a weak decline in T_m until becoming T_1-limited. Cooling from 40 K to 5 K, there is also a decline in T_m. Such a phenomenon has been noted in other V(IV) systems. In one example, such a decline was postulated to result from low-temperature tunneling of methyl rotations in alkyl ammonium counterions to the V(IV) complex.[32] VOPc and TiOPc lack methyl

groups or similarly fluxional moieties, so the observation of this low-temperature phenomenon may require further consideration.

Orientation Dependence of T_1 and T_m in CuPc

Analogous to the VOPc/TiOPc dilutions, we chose to study CuPc in a dilute diamagnetic matrix by preparing CuPc/ZnPc-doped samples at 1:1000 and 1:100 concentrations. The CuPc/ZnPc samples were prepared by dissolving the respective metal phthalocyanines in concentrated H_2SO_4, followed by reprecipitation over ice. Previous reports used this method to selectively generate the α-CuPc polymorph.[40] However, the PXRD patterns observed for CuPc/ZnPc samples do not strictly match reported diffraction patterns for either α- or β-CuPc.[41,42]

We collected the T_1 and T_m relaxation times at four field positions and observed similar temperature-dependent behavior at each field. At 5 K, the T_1 and T_m collected on the 1:1000 sample exhibit dependence on the field position – T_1's of 160 ms (306 mT), 83 ms (329 mT), 15 ms (339 mT), and 51 ms (342 mT); T_m's of 4.4 μs (306 mT), 10 μs (329 mT), 0.6 μs (339 mT), and 4.9 μs (342 mT). The spread in relaxation times is apparently larger at low temperature than what was observed for VOPc, with the relaxation times recorded at 339 mT being shortest consistently for the CuPc sample. Upon increasing the temperature above 30 K, the T_1's coalesce across the field positions to roughly similar values. T_m then becomes T_1 limited at 150 K with a value around 400 ns. The decreased T_1 time of the 339 mT feature relative to the other field positions may be due to greater contributions of the organic radical to relaxation pathways as evidenced by the changing intensity of the radical feature with increased temperature in the EDFS and higher relative concentration compared to the 1:100 sample. In the 1:100 CuPc/ZnPc sample, the T_1's are on average shorter than those for the 1:1000 sample by nearly an order of magnitude

from 5 to 50 K. The T_1's collected on the 1:100 sample then follow a similar trend in values compared to the 1:1000 sample at higher temperatures.

As discussed for VOPc, T_m is sensitive to the alignment of the principal axes of the spin with the external field of the spectrometer. CuPc exhibits resonances at noncanonical orientations, leading to anisotropy larger than the microwave quantum of X-band (~0.3 cm^{-1}) and Q-band (~1.1 cm^{-1}). There is also strong nitrogen superhyperfine structure resulting from the coordinating nitrogens in the phthalocyanine ring. Furthermore, the organic radical contributes to signal at 339 mT in the midst of the Cu electron spin transitions, whereas for VOPc the radical feature was more isolated from the vandyl spin transitions. As a result of these factors, strict assignment of orientation and hyperfine eigenvalues at a given field position is challenging.

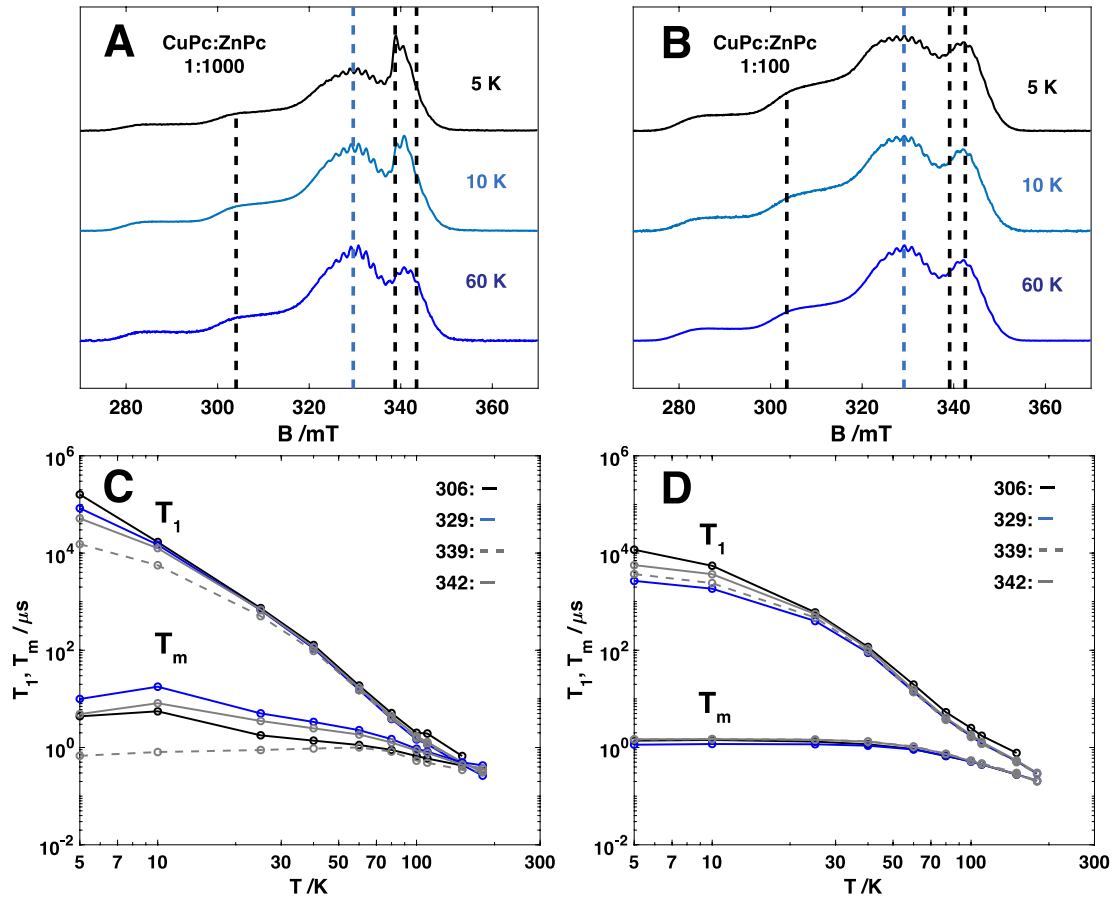

Figure 3.4 Echo-detected EPR X-band field sweeps of CuPc/ZnPc (**A**) 1:1000 and (**B**) 1:100 at 5, 10, and 60 K. Dashed lines indicate field positions where relaxation data were obtained. Comparison between the field-position-dependent behavior of the T_1 and T_M relaxation times for 5 – 180 K for CuPc/ZnPc (**C**) 1:1000 and (**D**) 1:100.

Frequency Dependence of T_1 and T_m in CuPc

We made Q-band EDFS T_1 and T_m measurements on the CuPc samples to compare to those collected at X-band. The position of maximum echo intensity in the EDFS in the 1:100 sample shifts to slightly higher field positions with increasing temperature. The organic radical feature appears in the spectra centered at 1218 mT. The relative intensities of this organic radical feature and the CuPc signal change over the temperature range and is likely due to changes in the total

integrated Cu signal intensity and the shot repetition time (SRT) used for the experiments. The separation of the radical signal from those arising from CuPc is more significant at Q-band than at X-band, but may still reflect the lower T_1's recorded at 1188 and 1190 mT at low temperatures compared to the analogous 339 and 334 mT positions at X-band (Figure 3.4). At approximately 25 K, the T_1 times recorded at X-band and Q-band become roughly the same. At low temperatures, the T_1's measured at X-band are generally longer than those measured at Q-band. This is consistent with the expected frequency dependence of the direct process as discussed for VOPc.

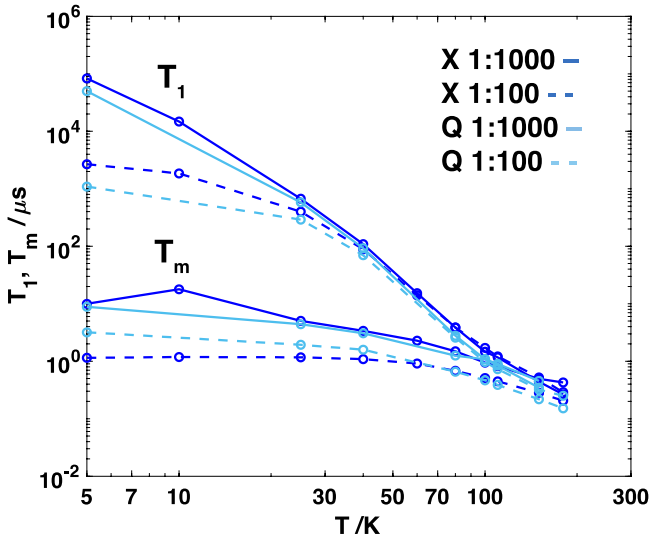

Figure 3.5 Comparison between the T_1 and T_M times vs. temperature for the 329 and 1188 mT features in CuPc at X-band and Q-band, respectively, for the 1:1000 and 1:100 preprarations.

The similar T_1 and T_m trends in temperature were observed regardless of sample concentration or microwave frequency, which suggests that the organic radical is likely not the dominant factor contributing to the different relaxation times between VOPc and CuPc. It is possible that the CuPc/ZnPc samples are influenced by the nonuniform polymorph distribution

observed by PXRD. To that end, we prepared a separate CuPc/ZnPc sample following the procedures used for VOPc/TiOPc samples (DCM/CF_3CO_2H/IPA) as discussed in Appendix B. In this sample, we observe similar T_1 and T_m times and temperature dependent trends, suggesting that the sample preparation and polymorph does not strongly change the observed relaxation.

Temperature Dependence of T_1 in CuPc

We fit the temperature-dependent spin-lattice relaxation rates measured in the 1:1000 CuPc/ZnPc sample at 329 mT to a direct, Raman, and local mode process as we did for VOPc. We found a direct process coefficient $A_{dir} = 2\ K^{-1}\ s^{-1}$, Raman coefficient $B_{ram} = 2.7 \times 10^5\ s^{-1}$ and Debye temperature $\theta_D = 112.8$ K, local mode coefficient $C_{loc} = 6.2 \times 10^6\ s^{-1}$ and average mode equivalent temperature $\Delta_{loc} = 272.1$ K (Table 1). This is consistent with what has been observed for CuTTP doped in ZnTPP ($A_{dir} = 19.5\ K^{-1}\ s^{-1}$, $B_{ram} = 4.8 \times 10^5\ s^{-1}$, $\theta_D = 120$ K, $C_{loc} = 1.5 \times 10^6\ s^{-1}$, $\Delta_{loc} = 250$ K).[33] As with the VOPc data collection, we have few points at low temperatures, and the direct process coefficient should be taken as approximate.

Unlike VOPc, the spectral features of the EDFS in the CuPc samples change distinctly at X-band going from 5 K to 60 K, in particular for the 1:1000 sample. This is evident in the shape and relative intensities of the signals around 329 and 339 mT. As previously mentioned, this effect is presumably influenced by the organic radical at low temperatures, whereas the short SRTs employed during higher temperature experiments will tend to minimize contributions from long-lived radical relaxation. The T_m's observed in the 1:1000 sample are longer than those of the 1:100 sample by half an order of magnitude at low temperatures up to 150 K, but exhibit little to no temperature dependence.

As with VOPc and CuTTP, there is a low-temperature decline in T_m observed in the CuPc samples. For both CuPc samples, the maximum T_m is observed near 10 K with a distinct decline moving toward lower temperatures and a gradual decline with increasing temperature until T_m becomes T_1-limited at 150 K.[33,39] In both CuPc and VOPc, the lack of temperature dependence in T_m is consistent with the restricted mobility within doped matrices.[23,36]

Discussion

We compare the temperature-dependent relaxation behavior of VOPc and CuPc 1:1000 samples measured at 335.6 and 329 mT, respectively. While the T_1 and T_m times of CuPc are longer than those of VOPc at low temperature, CuPc decoherence times become T_1-limited by ~150 K and there is a steep dropoff. Ultimately, coherence lifetimes could not be obtained for the CuPc sample past 180 K. In comparison, the VOPc T_m times only become T_1-limited close to room temperature due to the more gradual decline in T_1 over the temperature range compared to CuPc. This speaks to stronger Raman- and local mode-induced spin-lattice relaxation in CuPc samples than in VOPc. This is reflected in the fits of our T_1 data as well. The coefficients found by the fitting procedure for Raman and local mode processes in CuPc are an order of magnitude larger than those obtained for VOPc (Table 1). We can consider this in the context of the relative spin-orbit coupling of VOPc and CuPc. The many-electron SOC constant ($\lambda=\pm\zeta/2S$) is significantly larger for Cu(II) (λ = -830 cm^{-1}) than for V(IV) (λ = 250 cm^{-1}).[43] The Raman and local mode processes directly reflect the differences in SOC strength; therefore, the increased magnitude of the SOC coefficient in CuPc leads to an increased sensitive to temperature for spin-lattice relaxation.[37]

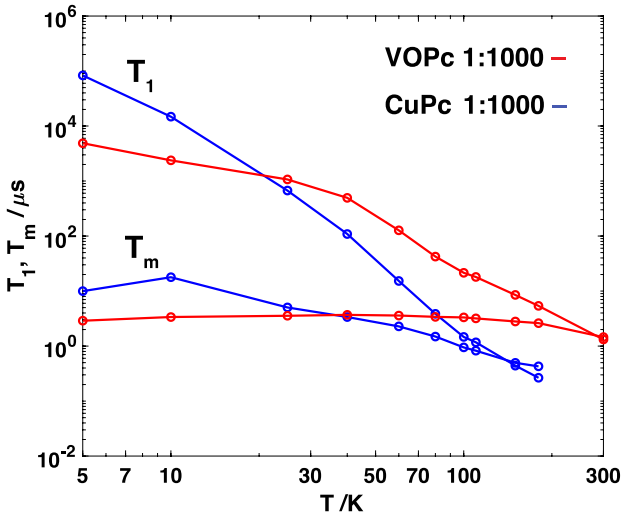

Figure 3.6 Comparison between X-band T_1's and T_M's vs. temperature for the 335.6 and 329 mT features in VOPc (red) and CuPc (blue), respectively.

We rationalize our observations based off literature precedent and ligand field theory.[18,44] Briefly, in C_{4v} or D_{4h} symmetry (appropriate for VOPc and CuPc respectively), a generalized expression for an S = ½ molecular g value from perturbation theory is given as:[45]

$$g_{mol} = g_e - \frac{n\lambda\alpha_1^2\beta_1^2}{\Delta E} \qquad Eq.3.1$$

Where g_e is the free-electron g value, ΔE is the energetic separation between the ground and a particular ligand field excited state, n is an integer constant, and β_1 and α_1 are coefficients reflecting covalencies between the d- and ligand-based orbitals in the ground and excited states, respectively. These parameters all contribute to the effective g value at a given orientation of the field with respect to the molecular frame. The static shift in molecular g values reflects the magnitude of SOC contributions to the ground state wavefunction. Modulation of SOC dominates the mechanisms of spin-lattice relaxation. As a result, the factors that minimize the impact of fluctuations of the SOC are implicit within the expression for g_{mol} such as increasing covalency,

increasing ΔE, or reducing λ. Such factors have previously been discussed by others in the field, such as Eaton et al., and inform our understanding of relaxation in these S = ½ systems. We will detail the three contributions below.

Ground state orbital angular momentum of a free ion is quenched by the introduction of a ligand field, removing degeneracy of the states. This quench is achieved in both C_{4v} and D_{4h} symmetries of VOPc and CuPc, respectively. By perturbational treatment of spin-orbit coupling, higher lying spin-orbital eigenfunctions of the zero-order Hamiltonian will be mixed (slightly) into the ground state wavefunction by an applied magnetic field due to terms in the perturbation Hamiltonian. This reintroduces orbital angular momentum contributions to the ground state observables, such as the g value. Indeed, this is the origin of Eq. 3.1. The greater the separation between excited state and ground state, the less that state will mix and contribute to the g shift (as seen in the inverse dependence of g_{mol} on ΔE. It is therefore important to consider the symmetry of the ground state wavefunction and the manifold of ligand-field excited states when considering transition metal electron spin qubit candidates. To the best of our knowledge, the specific ligand-field transitions contributing to the g values of CuPc and VOPc have not been specifically observed, likely due to the intense intraligand π-π* transitions that dominate the electronic absorption spectrum. The energies of the transitions that contribute to $g_{\|}$ were recently calculated to be similar in energy for CuPc and VOPc (22,165 and 22,745 cm^{-1}, respectively).[18] Thus, we would not expect the energetic separation of the ligand-field states to be the major contributor to the differential spin-lattice relaxation times in the V and Cu complexes regarded here. The energies of these excited states are also significantly higher than the Debye temperatures we calculated for CuPc (112.8 K/78 cm^{-1}) and VOPc (119.6 K/83 cm^{-1}), which affirms our decision not to include Orbach-type relaxation mechanisms into our model.

We next consider ligand-metal covalency. We expect the covalency to be significantly larger in CuPc relative to VOPc as the unpaired electron in CuPc lies in the $d_{x^2-y^2}$ orbital, which is oriented along the Cu-N bonds. In VOPc, the electron is located in d_{xy} and not along the V-N bond.

This is reflected experimentally in the observation of significant superhyperfine coupling between the electron spin and the ^{14}N nuclear spin (I = 1) on the $g_\perp$ features in CuPc EPR spectra with A(^{14}N) = [45-50, 40-48] MHz. We were unable to resolve ^{14}N superhyperfine structure in the EPR spectra of VOPc. The simulated line width (full-width at half-maximum) of VOPc is 1.5 mT (42 MHz at g = 2); this places an approximate upper bound on the four equivalently coupled ^{14}N hyperfine constants as A(^{14}N) < 10.5 MHz or less than a quarter than that observed in CuPc. Although increased covalency should benefit prolonged spin-lattice relaxation times, we observe more significant phonon/vibrational mode-mediated relaxation with increased temperature in CuPc relative to VOPc. It may be the case then that despite the more covalent Cu-ligand interaction, the magnitude of the SOC constant in Cu remains a large contributor to spin-lattice relaxation.

Finally, we will touch on hyperfine-mediated spin-lattice and phase memory relaxation. CuTTP was demonstrated to have similar Cu (~630 MHz) hyperfine and (~43 MHz) superhyperfine coupling constants to those we observe for CuPc (~650 and ~45 MHz for Cu and N, respectively). Single crystal and powder studies of CuTTP doped into ZnTTP have previously shown that the observed T_1 times are independent of orientation and insensitive to the contributions from ligand superhyperfine, which further supports the importance of the SOC coupling constant to the temperature dependence of the relaxation times.[23,35]

Conclusions

In summary, CuPc exhibits order of magnitude longer T_1 times than VOPc at low temperatures (5 K). However, the T_1 times decline more rapidly with increasing temperature in CuPc than in VOPc, which we attribute to more significant contributions of Raman and local vibrational mode relaxation pathways. In line with this, the T_m times become T_1-limited in CuPc around 150 K and coherence cannot even be detected past 180 K, whereas the T_1-limiting regime occurs near 300 K for VOPc. As mentioned, the goal for molecular qubit candidates is to produce qubits that exhibit long coherence times (>100 μs) at high temperatures. The T_m time is largely temperature-independent until becoming limited by T_1. So, consideration must go to both increasing the T_m time of a given qubit candidate (which can be accomplished by removing nuclear spins as a source of spin flip-flop or hyperfine-mediated relaxation) as well as to extending the T_1 time at higher temperatures to allow for coherence to be observed (which can be considered by taking into account symmetry and spin-orbit interaction).

Citations

(1) DiVincenzo, D. P. The Physical Implementation of Quantum Computation. *Fortschritte der Physik* **2000**, *48* (9–11), 771–783. https://doi.org/10.1002/1521-3978(200009)48:9/11<771::AID-PROP771>3.0.CO;2-E.

(2) Clarke, J.; Wilhelm, F. K. Superconducting Quantum Bits. *Nature* **2008**, *453* (7198), 1031–1042. https://doi.org/10.1038/nature07128.

(3) Atzori, M.; Sessoli, R. The Second Quantum Revolution: Role and Challenges of Molecular Chemistry. *J. Am. Chem. Soc.* **2019**, *141* (29), 11339–11352. https://doi.org/10.1021/jacs.9b00984.

(4) Wasielewski, M. R.; Forbes, M. D. E.; Frank, N. L.; Kowalski, K.; Scholes, G. D.; Yuen-Zhou, J.; Baldo, M. A.; Freedman, D. E.; Goldsmith, R. H.; Goodson, T.; Kirk, M. L.; McCusker, J. K.; Ogilvie, J. P.; Shultz, D. A.; Stoll, S.; Whaley, K. B. Exploiting Chemistry and Molecular Systems for Quantum Information Science. *Nat Rev Chem* **2020**, *4* (9), 490–504. https://doi.org/10.1038/s41570-020-0200-5.

(5) Dolde, F.; Jakobi, I.; Naydenov, B.; Zhao, N.; Pezzagna, S.; Trautmann, C.; Meijer, J.; Neumann, P.; Jelezko, F.; Wrachtrup, J. Room-Temperature Entanglement between Single Defect Spins in Diamond. *Nature Phys* **2013**, *9* (3), 139–143. https://doi.org/10.1038/nphys2545.

(6) Hanson, R.; Gywat, O.; Awschalom, D. D. Room-Temperature Manipulation and Decoherence of a Single Spin in Diamond. *Phys. Rev. B* **2006**, *74* (16), 161203. https://doi.org/10.1103/PhysRevB.74.161203.
(7) Wang, J.-F.; Yan, F.-F.; Li, Q.; Liu, Z.-H.; Liu, H.; Guo, G.-P.; Guo, L.-P.; Zhou, X.; Cui, J.-M.; Wang, J.; Zhou, Z.-Q.; Xu, X.-Y.; Xu, J.-S.; Li, C.-F.; Guo, G.-C. Coherent Control of Nitrogen-Vacancy Center Spins in Silicon Carbide at Room Temperature. *Phys. Rev. Lett.* **2020**, *124* (22), 223601. https://doi.org/10.1103/PhysRevLett.124.223601.
(8) Widmann, M.; Lee, S.-Y.; Rendler, T.; Son, N. T.; Fedder, H.; Paik, S.; Yang, L.-P.; Zhao, N.; Yang, S.; Booker, I.; Denisenko, A.; Jamali, M.; Momenzadeh, S. A.; Gerhardt, I.; Ohshima, T.; Gali, A.; Janzén, E.; Wrachtrup, J. Coherent Control of Single Spins in Silicon Carbide at Room Temperature. *Nature Mater* **2015**, *14* (2), 164–168. https://doi.org/10.1038/nmat4145.
(9) Herbschleb, E. D.; Kato, H.; Maruyama, Y.; Danjo, T.; Makino, T.; Yamasaki, S.; Ohki, I.; Hayashi, K.; Morishita, H.; Fujiwara, M.; Mizuochi, N. Ultra-Long Coherence Times amongst Room-Temperature Solid-State Spins. *Nat Commun* **2019**, *10* (1), 3766. https://doi.org/10.1038/s41467-019-11776-8.
(10) Sproules, S. Molecules as Electron Spin Qubits. In *Electron Paramagnetic Resonance*; 2016; pp 61–97. https://doi.org/10.1039/9781782629436-00061.
(11) Graham, M. J.; Zadrozny, J. M.; Shiddiq, M.; Anderson, J. S.; Fataftah, M. S.; Hill, S.; Freedman, D. E. Influence of Electronic Spin and Spin–Orbit Coupling on Decoherence in Mononuclear Transition Metal Complexes. *J. Am. Chem. Soc.* **2014**, *136* (21), 7623–7626. https://doi.org/10.1021/ja5037397.
(12) Graham, M. J.; Krzyaniak, M. D.; Wasielewski, M. R.; Freedman, D. E. Probing Nuclear Spin Effects on Electronic Spin Coherence via EPR Measurements of Vanadium(IV) Complexes. *Inorg. Chem.* **2017**, *56* (14), 8106–8113. https://doi.org/10.1021/acs.inorgchem.7b00794.
(13) Tesi, L.; Lucaccini, E.; Cimatti, I.; Perfetti, M.; Mannini, M.; Atzori, M.; Morra, E.; Chiesa, M.; Caneschi, A.; Sorace, L.; Sessoli, R. Quantum Coherence in a Processable Vanadyl Complex: New Tools for the Search of Molecular Spin Qubits. *Chem. Sci.* **2016**, *7* (3), 2074–2083. https://doi.org/10.1039/C5SC04295J.
(14) Albino, A.; Benci, S.; Tesi, L.; Atzori, M.; Torre, R.; Sanvito, S.; Sessoli, R.; Lunghi, A. First-Principles Investigation of Spin–Phonon Coupling in Vanadium-Based Molecular Spin Quantum Bits. *Inorg. Chem.* **2019**, *58* (15), 10260–10268. https://doi.org/10.1021/acs.inorgchem.9b01407.
(15) Lunghi, A.; Sanvito, S. How Do Phonons Relax Molecular Spins? *Science Advances 5* (9), eaax7163. https://doi.org/10.1126/sciadv.aax7163.
(16) Escalera-Moreno, L.; Suaud, N.; Gaita-Ariño, A.; Coronado, E. Determining Key Local Vibrations in the Relaxation of Molecular Spin Qubits and Single-Molecule Magnets. *J. Phys. Chem. Lett.* **2017**, *8* (7), 1695–1700. https://doi.org/10.1021/acs.jpclett.7b00479.
(17) Atzori, M.; Tesi, L.; Benci, S.; Lunghi, A.; Righini, R.; Taschin, A.; Torre, R.; Sorace, L.; Sessoli, R. Spin Dynamics and Low Energy Vibrations: Insights from Vanadyl-Based Potential Molecular Qubits. *J. Am. Chem. Soc.* **2017**, *139* (12), 4338–4341. https://doi.org/10.1021/jacs.7b01266.
(18) Mirzoyan, R.; Hadt, R. G. The Dynamic Ligand Field of a Molecular Qubit: Decoherence through Spin–Phonon Coupling. *Phys. Chem. Chem. Phys.* **2020**, *22* (20), 11249–11265. https://doi.org/10.1039/D0CP00852D.

(19) Ariciu, A.-M.; Woen, D. H.; Huh, D. N.; Nodaraki, L. E.; Kostopoulos, A. K.; Goodwin, C. A. P.; Chilton, N. F.; McInnes, E. J. L.; Winpenny, R. E. P.; Evans, W. J.; Tuna, F. Engineering Electronic Structure to Prolong Relaxation Times in Molecular Qubits by Minimising Orbital Angular Momentum. *Nat Commun* **2019**, *10* (1), 3330. https://doi.org/10.1038/s41467-019-11309-3.

(20) Atzori, M.; Morra, E.; Tesi, L.; Albino, A.; Chiesa, M.; Sorace, L.; Sessoli, R. Quantum Coherence Times Enhancement in Vanadium(IV)-Based Potential Molecular Qubits: The Key Role of the Vanadyl Moiety. *J. Am. Chem. Soc.* **2016**, *138* (35), 11234–11244. https://doi.org/10.1021/jacs.6b05574.

(21) Fataftah, M. S.; Krzyaniak, M. D.; Vlaisavljevich, B.; Wasielewski, M. R.; Zadrozny, J. M.; Freedman, D. E. Metal–Ligand Covalency Enables Room Temperature Molecular Qubit Candidates. *Chem. Sci.* **2019**, *10* (27), 6707–6714. https://doi.org/10.1039/C9SC00074G.

(22) Weil, J. A.; Bolton, J. R. Basic Principles of Paramagnetic Resonance. In *Electron Paramagnetic Resonance*; John Wiley & Sons, Ltd, 2006; pp 1–35. https://doi.org/10.1002/9780470084984.ch1.

(23) Du, J.-L.; Eaton, G. R.; Eaton, S. S. Electron Spin Relaxation in Vanadyl, Copper(II), and Silver(II) Porphyrins in Glassy Solvents and Doped Solids. *Journal of Magnetic Resonance, Series A* **1996**, *119* (2), 240–246. https://doi.org/10.1006/jmra.1996.0079.

(24) Bonizzoni, C.; Ghirri, A.; Atzori, M.; Sorace, L.; Sessoli, R.; Affronte, M. Coherent Coupling between Vanadyl Phthalocyanine Spin Ensemble and Microwave Photons: Towards Integration of Molecular Spin Qubits into Quantum Circuits. *Sci Rep* **2017**, *7* (1), 13096. https://doi.org/10.1038/s41598-017-13271-w.

(25) Stepanow, S.; Mugarza, A.; Ceballos, G.; Moras, P.; Cezar, J. C.; Carbone, C.; Gambardella, P. Giant Spin and Orbital Moment Anisotropies of a Cu-Phthalocyanine Monolayer. *Phys. Rev. B* **2010**, *82* (1), 014405. https://doi.org/10.1103/PhysRevB.82.014405.

(26) Bader, K.; Winkler, M.; Slageren, J. van. Tuning of Molecular Qubits: Very Long Coherence and Spin–Lattice Relaxation Times. *Chem. Commun.* **2016**, *52* (18), 3623–3626. https://doi.org/10.1039/C6CC00300A.

(27) Warner, M.; Din, S.; Tupitsyn, I. S.; Morley, G. W.; Stoneham, A. M.; Gardener, J. A.; Wu, Z.; Fisher, A. J.; Heutz, S.; Kay, C. W. M.; Aeppli, G. Potential for Spin-Based Information Processing in a Thin-Film Molecular Semiconductor. *Nature* **2013**, *503* (7477), 504–508. https://doi.org/10.1038/nature12597.

(28) Van Vleck, J. H. Paramagnetic Relaxation and the Equilibrium of Lattice Oscillators. *Phys. Rev.* **1941**, *59* (9), 724–729. https://doi.org/10.1103/PhysRev.59.724.

(29) Van Vleck, J. H. Paramagnetic Relaxation Times for Titanium and Chrome Alum. *Phys. Rev.* **1940**, *57* (5), 426–447. https://doi.org/10.1103/PhysRev.57.426.

(30) Stevens, K. W. H. The Theory of Paramagnetic Relaxation. *Rep. Prog. Phys.* **1967**, *30* (1), 189–226. https://doi.org/10.1088/0034-4885/30/1/305.

(31) Orbach, R. On the Theory of Spin-Lattice Relaxation in Paramagnetic Salts. *Proc. Phys. Soc.* **1961**, *77* (4), 821–826. https://doi.org/10.1088/0370-1328/77/4/301.

(32) Lin, C.-Y.; Ngendahimana, T.; Eaton, G. R.; Eaton, S. S.; Zadrozny, J. M. Counterion Influence on Dynamic Spin Properties in a V(IV) Complex. *Chem. Sci.* **2019**, *10* (2), 548–555. https://doi.org/10.1039/C8SC04122A.

(33) Zhou, Y.; Bowler, B. E.; Eaton, G. R.; Eaton, S. S. Electron Spin Lattice Relaxation Rates for S = 12 Molecular Species in Glassy Matrices or Magnetically Dilute Solids at Temperatures between 10 and 300 K. *Journal of Magnetic Resonance* **1999**, *139* (1), 165–174. https://doi.org/10.1006/jmre.1999.1763.
(34) Zhou, Y.; Bowler, B. E.; Eaton, G. R.; Eaton, S. S. Electron Spin Lattice Relaxation Rates for S = 12 Molecular Species in Glassy Matrices or Magnetically Dilute Solids at Temperatures between 10 and 300 K. *Journal of Magnetic Resonance* **1999**, *139* (1), 165–174. https://doi.org/10.1006/jmre.1999.1763.
(35) Du, J.-L.; More, K. M.; Eaton, S. S.; Eaton, G. R. Orientation Dependence of Electron Spin Phase Memory Relaxation Times in Copper(II) and Vanadyl Complexes in Frozen Solution. *Israel Journal of Chemistry* **1992**, *32* (2–3), 351–355. https://doi.org/10.1002/ijch.199200041.
(36) Eaton, S. S.; Harbridge, J.; Rinard, G. A.; Eaton, G. R.; Weber, R. T. Frequency Dependence of Electron Spin Relaxation for ThreeS = 1/2 Species Doped into Diamagnetic Solid Hosts. *Appl. Magn. Reson.* **2001**, *20* (1), 151–157. https://doi.org/10.1007/BF03162316.
(37) Eaton, S. S.; Eaton, G. R. Relaxation Times of Organic Radicals and Transition Metal Ions. In *Distance Measurements in Biological Systems by EPR*; Berliner, L. J., Eaton, G. R., Eaton, S. S., Eds.; Springer US: Boston, MA, 2000; pp 29–154. https://doi.org/10.1007/0-306-47109-4_2.
(38) Nagarajan, V.; Müller, B.; Storcheva, O.; Köhler, K.; Pöppl, A. Structure and Bonding of [VIVO(Acac)2] on the Surface of AlF3 as Studied by Pulsed Electron Nuclear Double Resonance and Hyperfine Sublevel Correlation Spectroscopy. *Phys. Chem. Chem. Phys.* **2009**, *11* (31), 6849–6854. https://doi.org/10.1039/B903826B.
(39) Atzori, M.; Tesi, L.; Morra, E.; Chiesa, M.; Sorace, L.; Sessoli, R. Room-Temperature Quantum Coherence and Rabi Oscillations in Vanadyl Phthalocyanine: Toward Multifunctional Molecular Spin Qubits. *J. Am. Chem. Soc.* **2016**, *138* (7), 2154–2157. https://doi.org/10.1021/jacs.5b13408.
(40) Abkowitz, M.; Chen, I.; Sharp, J. H. Electron Spin Resonance of the Organic Semiconductor, A-Copper Phthalocyanine. *J. Chem. Phys.* **1968**, *48* (10), 4561–4567. https://doi.org/10.1063/1.1668028.
(41) Hoshino, A.; Takenaka, Y.; Miyaji, H. Redetermination of the Crystal Structure of α-Copper Phthalocyanine Grown on KCl. *Acta Cryst B* **2003**, *59* (3), 393–403. https://doi.org/10.1107/S010876810300942X.
(42) Schmidt, M. U. Polycyclic Pigments. In *Industrial Organic Pigments*; John Wiley & Sons, Ltd, 2004; pp 421–566. https://doi.org/10.1002/3527602429.ch3.
(43) Figgis, B. N. *Introduction to Ligand Fields*; Interscience Publishers: New York, 1966.
(44) Shrivastava, K. N. Lattice-Dynamical Contributions to g-Values. *J. Phys. C: Solid State Phys.* **1982**, *15* (18), 3869–3876. https://doi.org/10.1088/0022-3719/15/18/005.
(45) Solomon, E. I. Introduction. *Comments on Inorganic Chemistry* **1984**, *3* (5), 227–229. https://doi.org/10.1080/02603598408080072.